

Mass distribution in nearby Abell clusters

E. L. Lokas,^{1*} R. Wojtak,² S. Gottlöber,³ G. A. Mamon^{4,5} and F. Prada⁶

¹ Nicolaus Copernicus Astronomical Center, Bartycka 18, 00-716 Warsaw, Poland

² Astronomical Observatory, Jagiellonian University, Orla 171, 30-244 Cracow, Poland

³ Astrophysikalisches Institut Potsdam, An der Sternwarte 16, 14482 Potsdam, Germany

⁴ Institut d’Astrophysique de Paris (UMR 7095: CNRS and Université Pierre & Marie Curie), 98 bis Bd Arago, F-75014 Paris, France

⁵ GEPI (UMR 8111: CNRS and Université Denis Diderot), Observatoire de Paris, F-92195 Meudon, France

⁶ Instituto de Astrofísica de Andalucía (CSIC), Apartado Correos 3005, E-18080 Granada, Spain

19 June 2019

ABSTRACT

We study the mass distribution in six nearby ($z < 0.06$) relaxed Abell clusters of galaxies A0262, A0496, A1060, A2199, A3158 and A3558. Given the dominance of dark matter in galaxy clusters we approximate their total density distribution by the NFW formula characterized by virial mass and concentration. We also assume that the anisotropy of galactic orbits is reasonably well described by a constant and that galaxy distribution traces that of the total density. Using the velocity and position data for 120–420 galaxies per cluster we calculate, after removal of interlopers, the profiles of the lowest-order even velocity moments, dispersion and kurtosis. We then reproduce the velocity moments by jointly fitting the moments to the solutions of the Jeans equations. Including the kurtosis in the analysis allows us to break the degeneracy between the mass distribution and anisotropy and constrain the anisotropy as well as the virial mass and concentration. The method is tested in detail on mock data extracted from N -body simulations of dark matter haloes. We find that the best-fitting galactic orbits are remarkably close to isotropic in most clusters. Using the fitted pairs of mass and concentration parameters for the six clusters we conclude that the trend of decreasing concentration for higher masses found in cosmological N -body simulations is consistent with the data. By scaling the individual cluster data by mass we combine them to create a composite cluster with 1465 galaxies and perform a similar analysis on such sample. The estimated concentration parameter then lies in the range $1.5 < c < 14$ and the anisotropy parameter in the range $-1.1 < \beta < 0.5$ at the 95 percent confidence level.

Key words: galaxies: clusters: general – galaxies: clusters: individual: A0262, A0496, A1060, A2199, A3158, A3558 – galaxies: kinematics and dynamics – cosmology: dark matter

1 INTRODUCTION

Studies of galaxy kinematics in clusters remain a major tool in determining the mass distribution in these objects, complemented by methods based on the analysis of the hot X-ray gas and gravitational lensing. Due to a limited number of measured galaxy redshifts per cluster such analyses have been usually performed on composite clusters by combining data from many objects (e.g. Carlberg et al. 1997; van der Marel et al. 2000; Biviano & Girardi 2003; Mahdavi & Geller 2004; Katgert, Biviano & Mazure 2004; Biviano & Katgert 2004; Goto 2005). The normalizations needed in stacking

the clusters together reduce however the number of parameters that can be estimated from the analysis. Besides, such studies are usually restricted to the analysis of velocity dispersion profile with the simplifying assumption of isotropic galactic orbits.

In this study we attempt a kinematical analysis of six individual clusters which we supplement in the end by a similar procedure performed on a composite cluster created from the galaxies belonging to the six clusters. Our method relies on an extension of the usual Jeans formalism beyond the lowest-order velocity moment and including also the kurtosis of the line-of-sight velocity distribution (Lokas 2002; Lokas & Mamon 2003). The formalism has been successfully applied to study the dark matter distribution in the Coma cluster of galaxies by Lokas & Mamon (2003). It has been shown

* E-mail: lokas@camk.edu.pl

Table 1. Observational parameters of the clusters.

assigned number	cluster name	RA (J2000)	Dec (J2000)	redshift z	number of galaxies	velocity dispersion $\sigma_{\text{los}} [\text{km s}^{-1}]$	kurtosis κ_{los}
1	A0262	01 ^h 52 ^m 50.4 ^s	+36°08'46"	0.0163	120	527 ± 34	2.63 ± 0.44
2	A0496	04 ^h 33 ^m 37.1 ^s	-13°14'46"	0.0329	270	719 ± 31	3.36 ± 0.30
3	A1060	10 ^h 36 ^m 51.3 ^s	-27°31'35"	0.0126	330	696 ± 27	2.68 ± 0.27
4	A2199	16 ^h 28 ^m 37.0 ^s	+39°31'28"	0.0302	180	795 ± 42	2.49 ± 0.36
5	A3158	03 ^h 42 ^m 39.6 ^s	-53°37'50"	0.0597	145	970 ± 57	2.58 ± 0.40
6	A3558	13 ^h 27 ^m 54.8 ^s	-31°29'32"	0.0480	420	948 ± 33	2.70 ± 0.24

that, for a restricted class of dark matter distributions motivated by the results of cosmological N -body simulations, the joint analysis of velocity dispersion and kurtosis allows us to break the usual degeneracy between the mass distribution and velocity anisotropy and constrain the parameters of the dark matter profile. Recently we have tested the reliability of this approach against a series of N -body simulations (Sanchez, Lokas & Mamon 2004) and also applied it to constrain the dark matter distribution in the Draco dwarf spheroidal galaxy (Lokas, Mamon & Prada 2005a).

Here we farther test the method on a different set of cosmological N -body simulations by studying in detail the errors in the estimated parameters following from the sampling errors of velocity moments. We also introduce and test a new procedure of interloper removal which we then apply to the clusters. With a number of available galaxy redshifts per cluster much smaller than for Coma we had however to introduce a number of simplifications in our modelling compared to Lokas & Mamon (2003). We model the total mass distribution instead of only the dark matter component, we assume that galaxies trace the total mass distribution and we use the velocity data of all galaxies, not only ellipticals. On the other hand, we believe that the carefully selected clusters studied here are much more relaxed compared to Coma and therefore we avoid any uncertainties due to departures from dynamical equilibrium.

The paper is organized as follows. In Section 2 we briefly describe our data set. In Section 3 we summarize our method of data modelling including the removal of interlopers and fitting of velocity moments and test it on a sample of dark matter haloes extracted from a cosmological N -body simulation. The results for the six galaxy clusters and the composite cluster are presented in Section 4. The discussion follows in Section 5.

2 THE DATA

We have searched the NASA/IPAC Extragalactic Database (NED) for nearby ($z < 0.1$) well-studied galaxy clusters with at least 120 galaxies within projected distance of about 2 Mpc from the cluster centre and with cz velocities differing from the cluster mean by less than $\pm 4000 \text{ km s}^{-1}$. Among a few tens of clusters selected in this way we have chosen those which are likely to be relaxed judging by the regularity of their X-ray surface brightness maps obtained with Einstein (Jones & Forman 1999) and ASCA (Horner et al. 2000) satellites. Next we have looked at the regularity of the diagrams showing the line-of-sight velocities of galaxies as a

function of projected distance from the cluster centre. We have rejected those with irregular diagrams which may indicate merging or presence of neighbouring structures (Lokas et al. 2005b) for which our method of interloper removal does not work.

Table 1 lists the clusters we chose for the analysis together with their positions and redshifts as given by NED. We also give the number of galaxies per cluster used for the calculation of the velocity moments. The last two columns give the values of the line-of-sight velocity moments, dispersion and kurtosis calculated for all galaxies. The method of estimating these values is discussed in the next section. The list includes some very well known clusters. A0496 was studied in detail by Durret et al. (2000) who called it a prototype of a relaxed cluster. Indeed the cluster seems to have the most regular X-ray luminosity distribution of those in our sample and a single central galaxy whose position coincides with the centre of the gas distribution. The cluster A1060 (Hydra I, Fitchett & Merritt 1988), although quite similar to A0496 in many aspects, has two central galaxies and somewhat less uniform X-ray distribution so it may have just reached equilibrium after a major merger. None of the clusters, however, is completely free of substructure or neighbours (even A0496). A3558 (Shapley 8) is the richest member of the Shapley supercluster (Dantas et al. 1997; Bardelli et al. 1998) including a much smaller neighbour A3556 and a bigger, more distant cluster A3562. For this cluster we have restricted the analysis to distances where members of A3556 and A3562 are not likely to contaminate the sample. A2199 seems to be quite a relaxed cluster but has a less massive neighbour A2197 and other groups which made us restrict the analysis to distances much smaller than the estimated virial radius. Also A0262, a member of the Perseus-Pisces supercluster, can be affected by neighbouring structures.

It is generally believed that elliptical galaxies in clusters comprise a virialized, more relaxed subsample compared to (late) spirals which might be infalling into the cluster for the first time. It could therefore be desirable to restrict the analysis to ellipticals as was done in the case of Coma cluster by Lokas & Mamon (2003). However, for the present sample of clusters the morphological information is available only for a small fraction of galaxies making such an analysis impossible. Given a larger number of galaxies per cluster one could also attempt to measure their surface density distribution reliably and use it as an input in the kinematical analysis. With scarce samples presently available we are forced to assume that the number density of galaxies follows the total density distribution.

For the kinematical analysis we have chosen as the cen-

tres of the clusters their central cD galaxies which coincide with the centre of the X-ray surface brightness distribution. In the case of the presence of two central galaxies (in A1060 and A3158) we have chosen as a centre the position of the one which is closer to the centre of the X-ray surface brightness distribution. The galaxy velocities have been transformed to the reference frame of the cluster and in order to calculate the distances within clusters we have transformed the cluster velocities to the reference frame of the cosmic microwave background.

3 THE METHOD

3.1 Overview of the method

In this section we summarize our method of determining the mass distribution from velocity moments, as developed in Łokas (2002) and Łokas & Mamon (2003), and test it against mock data obtained from N -body simulations. The method relies on fitting the solutions of the Jeans equations for the second and fourth velocity moments to the profiles of the moments determined from the data. For the velocity dispersion projected along the line of sight, σ_{los} , the Jeans formalism gives (Binney & Mamon 1982)

$$\sigma_{\text{los}}^2(R) = \frac{2}{I(R)} \int_R^\infty \frac{\nu \sigma_r^2 r}{\sqrt{r^2 - R^2}} \left(1 - \beta \frac{R^2}{r^2}\right) dr, \quad (1)$$

where $\nu(r)$ and $I(R)$ are the 3D and the surface distribution of the tracer as a function of a true (r) and projected (R) distance from the object centre respectively. The parameter

$$\beta = 1 - \frac{\sigma_\theta^2(r)}{\sigma_r^2(r)} \quad (2)$$

describes a relation between the angular σ_θ and radial σ_r velocity dispersions and characterizes the anisotropy of the tracer orbits. We will assume it here to be constant with radius and consider $-\infty < \beta \leq 1$ which covers all interesting possibilities from radial orbits ($\beta = 1$) to isotropy ($\beta = 0$) and circular orbits ($\beta \rightarrow -\infty$). For constant β the radial velocity dispersion, $\sigma_r(r)$ in equation (1) is

$$\nu \sigma_r^2(r) = r^{-2\beta} \int_r^\infty r^{2\beta} \nu \frac{d\Phi}{dr} dr \quad (3)$$

where Φ is the gravitational potential.

For the fourth projected velocity moment we have

$$\overline{v_{\text{los}}^4}(R) = \frac{2}{I(R)} \int_R^\infty \frac{\nu \overline{v_r^4} r}{\sqrt{r^2 - R^2}} g(r, R, \beta) dr \quad (4)$$

where $g(r, R, \beta) = 1 - 2\beta R^2/r^2 + \beta(1 + \beta)R^4/(2r^4)$ and

$$\nu \overline{v_r^4}(\beta = \text{const}) = 3r^{-2\beta} \int_r^\infty r^{2\beta} \nu \sigma_r^2(r) \frac{d\Phi}{dr} dr. \quad (5)$$

In the following we will rescale the fourth moment to obtain the line-of-sight or projected kurtosis

$$\kappa_{\text{los}}(R) = \frac{\overline{v_{\text{los}}^4}(R)}{\sigma_{\text{los}}^4(R)} \quad (6)$$

whose value is 3 for a Gaussian distribution.

Having measured the line-of-sight velocities and projected positions for a number of tracer particles or galaxies one can estimate the profiles of velocity dispersion and

kurtosis by taking n tracer particles per bin and using the following estimators of variance and kurtosis

$$S^2 = \frac{1}{n} \sum_{i=1}^n (v_i - \bar{v})^2 \quad (7)$$

and

$$K = \frac{\frac{1}{n} \sum_{i=1}^n (v_i - \bar{v})^4}{(S^2)^2} \quad (8)$$

where

$$\bar{v} = \frac{1}{n} \sum_{i=1}^n v_i \quad (9)$$

is the mean of velocities in a bin. Since in the case of study of galaxy kinematics in clusters the number of galaxies usually does not exceed a few hundred, and for our least sampled cluster in Table 1 (A0262) is as low as 120, in order to have at least 4 data points in each of the velocity dispersion or kurtosis profiles we need to adopt a rather low number of $n = 30$ objects per bin. Using the Monte Carlo method described in the Appendix of Łokas & Mamon (2003) one can then construct unbiased and Gaussian-distributed estimators of line-of-sight velocity dispersion s and kurtosis-like variable k

$$s = \left(\frac{n}{n-1} S^2 \right)^{1/2} \quad (10)$$

$$k = \left[\log \left(\frac{3}{2.68} K \right) \right]^{1/10} \quad (11)$$

where S and K are given by equations (7)-(9). The factor $n-1$ in equation (10) is the well known correction for bias when estimating the sample variance, valid independently of the underlying distribution. In (11) the factor 3/2.68 corrects for the bias in the kurtosis estimate, i.e. unbiased estimate of kurtosis is $K' = 3K/2.68$, while the rather complicated function of K' assures that the sampling distribution of k is approximately Gaussian. We have also checked that defined in this way the measured velocity dispersion and kurtosis in a given bin are very weakly correlated so the data points can be fitted as independent. The standard errors in the case of s are $s/\sqrt{2(n-1)}$ while in the case of k are approximately 0.02 (for $n \approx 30$). In the following we assign these sampling errors to our mock and real data points.

We will further assume that the total density distribution in the studied objects (simulated haloes or galaxy clusters) and the distribution of the tracer are well approximated up to the virial radius r_v by the NFW formula (Navarro, Frenk & White 1997)

$$\frac{\rho(s)}{\rho_{c,0}} = \frac{\Delta_c c^2 g(c)}{3 s (1+cs)^2}, \quad (12)$$

where $s = r/r_v$, $\rho_{c,0}$ is the present critical density, $\Delta_c = 101.9$ is the characteristic density parameter, c is the concentration parameter and $g(c) = [\ln(1+c) - c/(1+c)]^{-1}$. We define the virial mass and radius as those with mean density $\Delta_c = 101.9$ times the critical density according to the spherical collapse model for the standard Λ CDM cosmology (see Łokas & Hoffman 2001). The surface distribution of the tracer $I(R)$ following from 3D density profile (12) can be found, together with other properties of the NFW haloes, in Łokas & Mamon (2001).

Having estimated the velocity dispersion and kurtosis profiles from the measured positions and velocities we can fit these data with the solutions (1)-(4) estimating three free parameters: the virial mass M_v , concentration c and anisotropy β . In the remaining part of this section we apply the method to a set of mock data in order to assess its viability in reproducing the properties of real galaxy clusters. Our approach here is similar to that of Sanchis et al. (2004), but in addition we address the problem of interlopers and we estimate the errors in the parameters due to sampling errors.

3.2 Removal of interlopers

For this work we used the results of a cosmological dark matter simulation described by Wojtak et al. (2005). The simulation was performed within a box of size $150 h^{-1}$ Mpc assuming the concordance cosmological model (Λ CDM) with parameters $\Omega_M = 0.3$, $\Omega_\Lambda = 0.7$, $h = 0.7$ and $\sigma_8 = 0.9$. We focused on 10 massive and isolated haloes extracted from the final output of the simulation whose properties are listed in Table 1 of Wojtak et al. (2005). In order to emulate the observations we place an observer at a distance of 100 Mpc from a centre of a given halo so that he will be able to see it receding with a velocity of around 7000 km s^{-1} . We assume that the line of sight is parallel to the x, y or z axis of the simulation box, with respect to which the haloes should be oriented randomly. The observer is located far enough from the halo so that the cone of observation can be approximated by a cylinder. We then project all particle velocities along the line of sight and the distances on the surface of the sky restricting the observations to the circle of projected radius $R = r_v$ on the sky. Next we reject all particles with velocities differing from the mean velocity of the halo by more than $\pm 4000 \text{ km s}^{-1}$, as we did for the real clusters. This cut-off corresponds to at least $4\sigma_{\text{los}}$ (with σ_{los} calculated for all particles in the halo) so it is not very restrictive. From the obtained sample of particles we randomly draw 300 out of about 10^4 per halo.

The velocities and positions of 300 particles obtained in this way for halo 1 (of mass $M_v = 7.5 \times 10^{14} M_\odot$ and virial radius $r_v = 2.3$ Mpc) observed along x, y and z axis (upper, middle and lower row respectively) are shown in Fig. 1. In the plots shown in the left column of the Figure the particles that happen to lie inside the virial radius of the halo (as verified using 3D information) were coded with filled circles, while those outside the virial radius are shown with open symbols. In the right panel the coding is similar but the particles were divided into those which are bound (have velocities smaller than the escape velocity, $v < v_{\text{esc}}$) or unbound to the halo. The axes along which the particles were observed are marked in the lower left corner of each panel together with the labels showing whether the distinction between the particles was made with the criterion of r_v or v_{esc} . In the upper left corners of the plots we give the numbers of particles fulfilling or not the criterion which sum to the total number of 300.

Averaging over 10 haloes and 3 directions of observation we find that of the total number of particles (300), 76 percent reside inside r_v , 87 percent inside $2r_v$, while 92 percent are actually bound to its halo. In addition, the unbound particles are always a subsample of those with $r > 2r_v$, i.e.

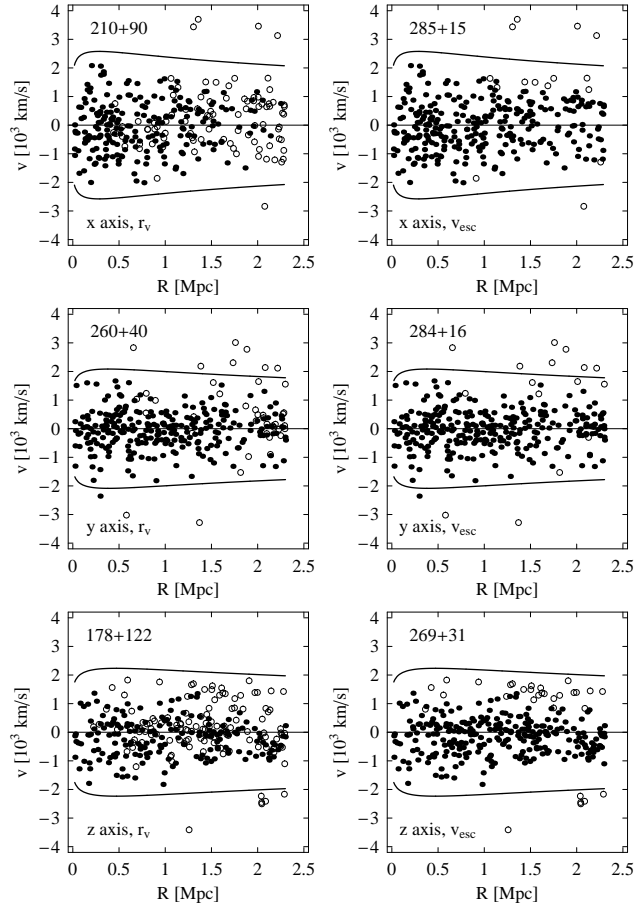


Figure 1. Line-of-sight velocities of 300 particles sampled from halo 1 as a function of projected distance from the centre of the halo. The upper, middle and lower row show observations performed along x, y and z axis of the simulation box respectively. Filled (empty) circles mark particles which actually reside inside (outside) r_v (left column) or which are bound (unbound) to the halo (right column). The numbers in the upper left corner of each panel give the numbers of filled+empty circles. Solid lines show fitted $\pm 3\sigma_{\text{los}}(R)$ profiles separating the particles included in the analysis from those rejected as interlopers.

there are no unbound particles inside $2r_v$. The particles that do not fulfill any of the criteria are more common at larger projected distances from the centre of the halo. The particles from outside r_v are obviously candidates for interlopers since they would not be used to estimate the density profile from the 3D information. However, as the cited numbers show, about half of them are actually close to the halo (within $2r_v$) and most of them are bound to the halo and therefore probably reasonably good tracers of the potential. This agrees with the recent studies based on N -body simulations (e.g. Klypin et al. 2003; Prada et al. 2005; Betancort-Rijo et al. 2005) which demonstrate that the virialized region extends somewhat beyond the virial radius, as we define it. Besides, the simulated dark matter haloes are usually not spherical and by imposing spherical symmetry in our definition of virialized region we may in fact cut out particles which are actually members of the halo. Anyway, most of the candidate interlopers reside close to the mean velocity of the

halo and only a few of them are true outliers which could significantly alter our estimates of the velocity moments.

We proceed to remove these outliers in the following way. First we calculate the velocity dispersion profiles by binning the data (with 30 particles per bin) and assigning them sampling errors, as described in the previous subsection. We then fit the data with solutions (1) assuming $\beta = 0$ and adjusting M_v and c . Although the β values of dark matter haloes are mildly radial (with mean $\beta \approx 0.3$, see e.g. Wojtak et al. 2005; Mamon & Lokas 2005) the actual values of the parameters are not very important at this stage since our purpose now is only to reproduce the shape of the dispersion profile and this can be done well with 2 parameters instead of 3. If the velocity dispersion increases strongly and the fit goes to values of $c < 1$ (the NFW profile would not make sense since the scale radius would be larger than the virial radius) we keep $c = 1$ and adjust M_v and β instead. We then reject all particles lying outside the mean velocity $\pm 3\sigma_{\text{los}}(R)$ where $\sigma_{\text{los}}(R)$ is the velocity dispersion profile obtained with our best-fitting parameters. The procedure is repeated until no more particles are removed. In each iteration we also calculate new estimate of the mean line-of-sight velocity of the particles with respect to which the rejection is performed.

The $\pm 3\sigma_{\text{los}}(R)$ profiles from the last iterations are shown as solid lines in Fig. 1. As we can see, the procedure removes the most obvious interlopers which affect the velocity moments most strongly. The mean number of particles removed in all 30 experiments is 14 which corresponds to 61 percent of the mean number of unbound particles per halo. In rare cases where the initial velocity dispersion profile from the data is strongly increasing the first fit may not remove any particles and it is necessary to repeat the fitting for a smaller number of data points. In such cases it may also happen that a member particle from the centre of the halo is removed. The effectiveness of the method will be compared to other methods of interloper removal used in the literature in a forthcoming paper (Wojtak et al., in preparation).

3.3 Fitting of velocity moments

We now assess the viability of our method by jointly fitting both velocity dispersion and kurtosis profiles calculated from our mock data for the simulated dark matter haloes. After removal of interlopers we are left with 8-9 data points for both dispersion and kurtosis which is of the same order as what we have for real galaxy clusters. The quality of the obtained fits and magnitude of errors in the parameters should therefore also be similar.

We jointly fit the mock data for velocity dispersion and kurtosis with the predictions from the Jeans formulae (1)-(6) adjusting the three parameters M_v , c and β . The parameters which minimize χ^2 are shown in Fig. 2 as filled dots for 10 haloes observed along x axis of the simulation box (for the observations along y and z axis the results are similar). The 1σ errors in the parameters due to the sampling errors, were found by exploring the 3-dimensional confidence region in the $M_v - \beta$, $\beta - c$ and $M_v - c$ parameter planes and finding probability contours corresponding to 1σ , 2σ and 3σ i.e. $\Delta\chi^2 = \chi^2 - \chi^2_{\text{min}} = 3.53, 8.02, 14.2$. The parameters of the haloes obtained from the full 3D information are marked as crosses. The masses and concentrations were taken from

Figure 2. Fitted parameters of the simulated dark matter haloes observed along the x axis of the simulation box. The three panels show from top to bottom the virial mass M_v (in units of $10^{14} M_\odot$), concentration c and the anisotropy parameter β . The filled dots show the parameters estimated from the joint fitting of velocity dispersion and kurtosis data with 1σ error bars. Crosses mark values estimated from the full 3D information.

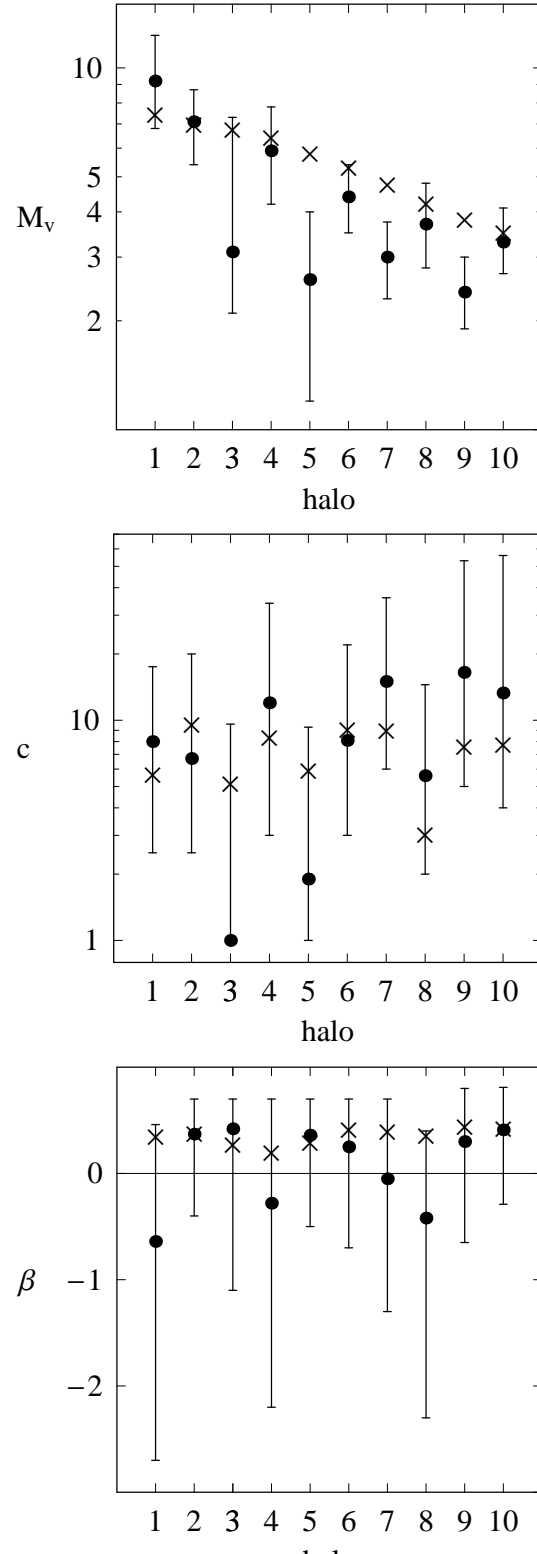


Table 1 of Wojtak et al. (2005) and the β parameters were calculated from the β profiles of the haloes by taking averages in 10 radial bins inside the virial radius.

The discrepancies between the fitted and true values of the parameters may be due to non-sphericity, presence of substructure, projected outliers and departures from equilibrium e.g. in the form of streaming motions. However, as we can see, the true values of the parameters are almost always within the estimated 1σ error bars of the fitted values (except for the mass estimates for haloes 5, 7 and 9 where the fitted values are somewhat lower). We conclude from this analysis that the sampling errors are the main source of error in this method.

We also note that quite probably the method works even better for real galaxies in clusters than for our randomly selected particles. Although it would be worthwhile to test the method on simulated galaxies, at the present stage of the simulations this would be reduced to using subhaloes detected with standard halo-finding techniques. The distributions of subhaloes both in space and velocity are known to be biased with respect to those of dark matter particles (Diemand et al. 2004) and probably still suffer from overmerging problem. The density distribution of subhaloes is flat in the centre while both the particles in simulated haloes and galaxies in clusters have cuspy profiles. It would be very difficult to disentangle the effects mentioned above from the uncertainties due to the use of subhaloes.

Besides, simulations including baryons suggest that clusters tend to be more spherical than pure dark matter haloes (Kazantzidis et al. 2004; Basilakos et al. 2005) which would reduce the projection effects due to non-sphericity of the systems. We also believe that cluster-cluster mergers can be more easily detected in real clusters than in a single final output of an N -body simulation of dark matter haloes by studies of the X-ray emitting gas and so our sample of clusters is probably more relaxed than the sample of dark matter haloes we studied. In the application of the method to real galaxy clusters we will therefore neglect other sources of errors and estimate the uncertainties in the parameters only from the sampling errors of the velocity moments.

4 RESULTS

4.1 Removal of interlopers

We now proceed to apply the method of joint fitting of velocity moments to the sample of six clusters listed in Table 1. We start by plotting in Fig. 3 the line-of-sight velocities of galaxies with respect to the cluster mean velocity as a function of projected distance from the cluster centre. In order to separate the galaxies which will be used in the calculation of velocity moments from the supposed interlopers we apply the procedure for interloper removal described in the previous section, exactly as we did for simulated data with the additional assumption that the tracer density is proportional to the total mass density (we do not infer the tracer density from the observed surface number density of galaxies, because the latter would be very uncertain for such small samples and probably suffers from incompleteness that varies with projected radius).

Since we do not a priori know the virial radius of the

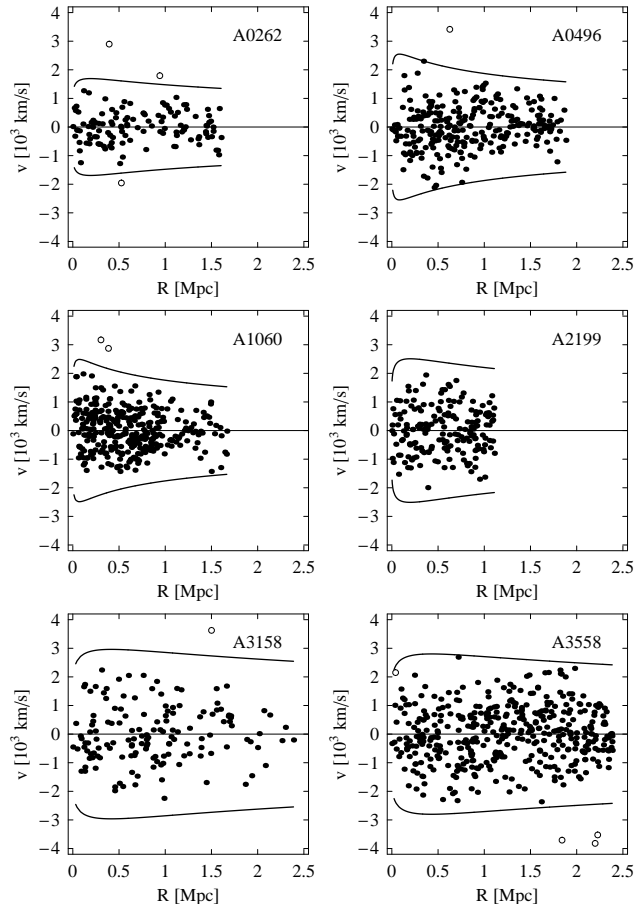


Figure 3. Line-of-sight velocities of galaxies with respect to the cluster mean velocity as a function of projected distance from the cluster centre for the six clusters listed in Table 1. Solid lines show fitted $\pm 3\sigma_{\text{los}}(R)$ profiles separating the galaxies included in the analysis (filled circles) from those rejected as interlopers (empty circles).

cluster, after estimating the virial mass in each iteration we check whether all fitted data points lie inside the virial radius or an additional data point could be included and adjust the number of points accordingly. The $\pm 3\sigma_{\text{los}}(R)$ profiles obtained in the final iteration of the procedure are shown as solid lines in Fig. 3. As can be read from the Figure the number of rejected galaxies is between 0 (for A2199) and 4 (for A3558), much lower than the number of particles rejected during the application of the method to simulated haloes.

Having found the final sample of galaxies we divide the data into radial bins of 30 galaxies (except for A3158 which has 29 galaxies per bin) and calculate the velocity dispersion and kurtosis profiles which are shown in Fig. 4 and 5 with 1σ sampling errors. We see that the profiles are similar to those characteristic for objects with NFW-like density profiles and orbits close to isotropic: the global trend is that both profiles slightly decrease with radius (see Lokas & Mamon 2001; Sanchis et al. 2004). A3558 shows the most variable velocity dispersion profile with one discrepant point at 0.7 Mpc (which is due to the single galaxy with discrepant velocity present in this bin – see Fig. 3) and a secondary increase at about 1.8 Mpc while its kurtosis profile remains

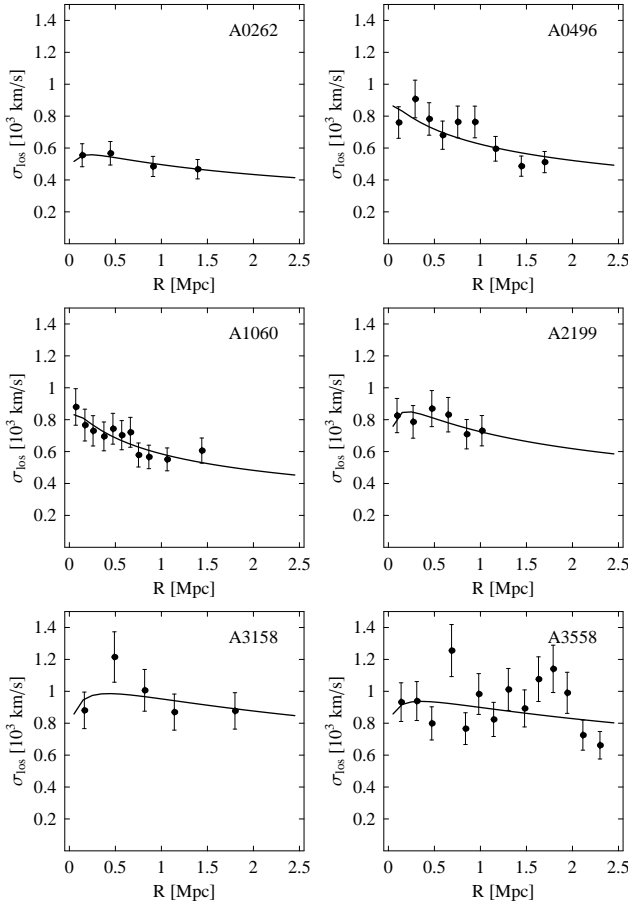


Figure 4. Line-of-sight velocity dispersion as a function of projected distance from the cluster centre for the six clusters. Solid lines show the best-fitting profiles with parameters listed in Table 2.

rather uniform. On the other hand A0496, believed to be a very relaxed cluster, has the most variable kurtosis profile. In an attempt to verify whether this variability may be due to departures from equilibrium e.g. in the form of the presence of infalling groups of galaxies we have also looked at the mean line-of-sight velocity profiles with respect to the cluster mean. They do not however depart strongly from zero, typically remaining in each bin within $0.2V_v$ (the circular velocity at the virial radius as determined in the next subsection).

4.2 Estimated parameters of the clusters

In the following analysis we assume that the galaxy distribution follows that of the total mass distribution. Although this assumption is far from obvious there is evidence from studies of clusters (e.g. Carlberg et al. 1997; Lokas & Mamon 2003; Biviano & Girardi 2003) that both number density and luminosity density of galaxies in clusters are cuspy and therefore can be quite well approximated by the NFW profile (contrary to the distribution of subhaloes in the dark matter simulations, which probably have a shallow core, see Diemand et al. 2004). The concentration of these distributions does not have to be the same as that of the total mass,

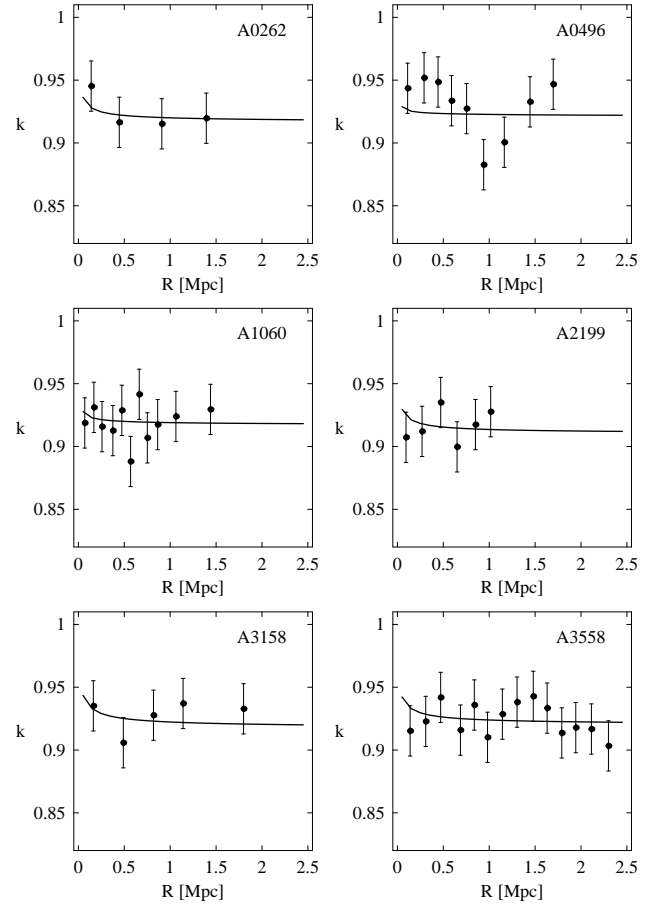


Figure 5. Line-of-sight kurtosis variables as function of projected distance from the cluster centre for the six clusters. Solid lines show the best-fitting profiles with parameters listed in Table 2.

Table 2. Fitted parameters of the clusters.

no.	cluster	M_v [$10^{14} M_\odot$]	c	β	χ^2/N
1	A0262	$2.7^{+1.2}_{-1.0}$	$4.2^{+11.3}_{-3.2}$	$-0.03^{+0.63}_{-2.27}$	1.1/5
2	A0496	$5.3^{+1.1}_{-1.1}$	$9.3^{+16.7}_{-6.3}$	$0.26^{+0.44}_{-0.79}$	18.5/15
3	A1060	$4.4^{+1.1}_{-1.0}$	$14.0^{+22.0}_{-10.0}$	$0.03^{+0.72}_{-1.13}$	8.6/19
4	A2199	$7.1^{+3.4}_{-2.4}$	$10.4^{+14.6}_{-7.9}$	$-0.55^{+1.05}_{-2.75}$	3.8/9
5	A3158	$15.4^{+7.6}_{-5.4}$	$3.5^{+7.5}_{-2.5}$	$0.004^{+0.55}_{-1.70}$	5.0/7
6	A3558	$12.5^{+3.5}_{-4.5}$	$2.7^{+5.3}_{-1.7}$	$0.15^{+0.35}_{-0.75}$	27.7/25

but with numbers of galaxies as low as 120 per cluster we are not able to reliably estimate the distribution of the tracer.

We jointly fitted the data for velocity dispersion and kurtosis with the predictions from the Jeans formulae (1)–(6) by minimizing χ^2 and adjusting the three parameters M_v , c and β . The best-fitting parameters for the six clusters are shown in Fig. 6 as filled dots together with 1σ

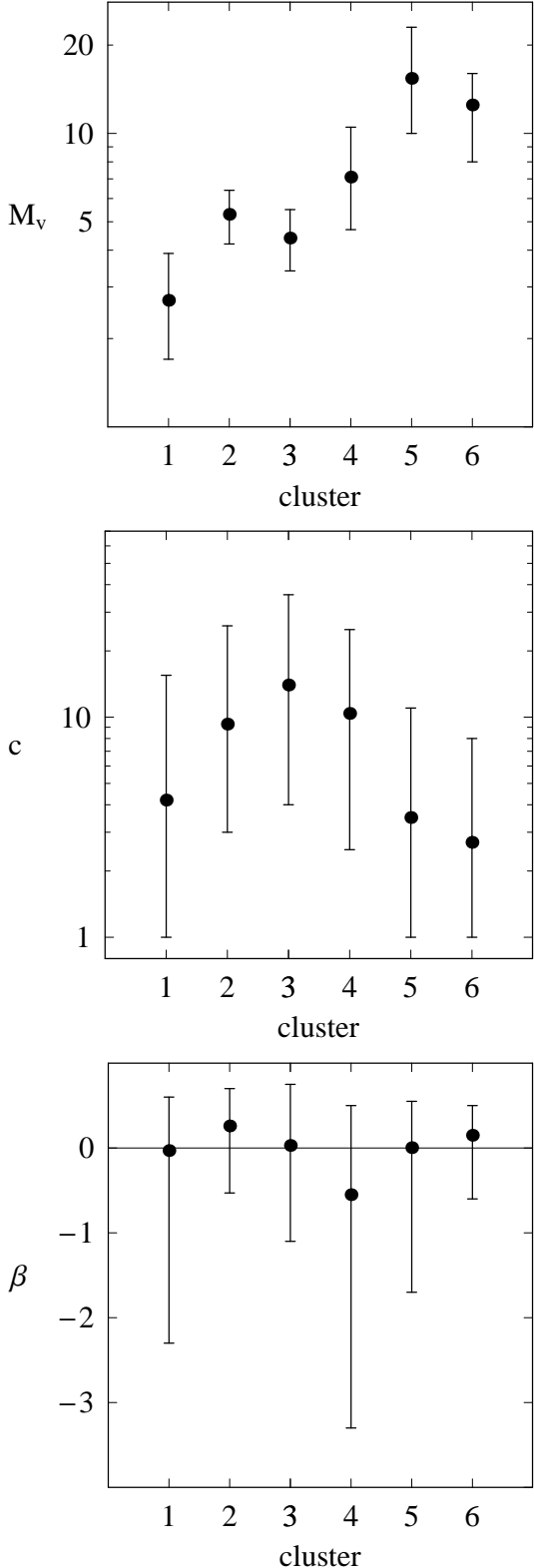


Figure 6. Fitted parameters of the clusters. The three panels show from top to bottom the virial mass M_v (in units of $10^{14} M_\odot$), concentration c and the anisotropy parameter β with 1σ error bars. The numbering of clusters is the same as in Table 1 and 2.

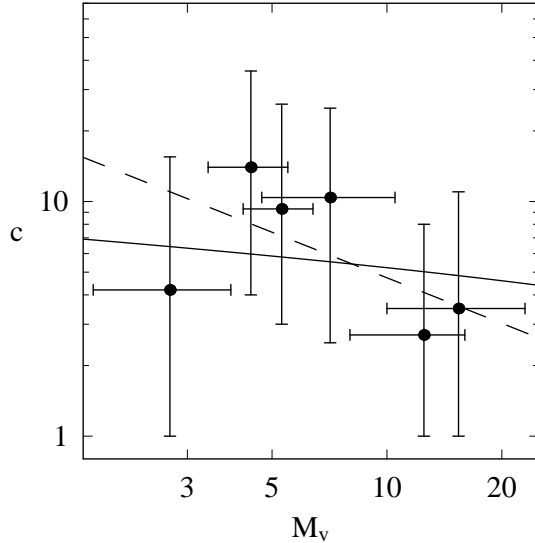


Figure 7. The mass-concentration relation. The filled circles show the best-fitting M_v - c pairs for the six clusters with 1σ error bars. M_v is given in units of $10^{14} M_\odot$. The solid line plots the prediction from the N -body simulations by Bullock et al (2001) while the dashed line shows the best fit to the data points.

error bars. The exact values are listed in Table 2 where the last column shows also the goodness of fit measure, χ^2/N . (The virial radii corresponding to the virial masses are $r_v = 1.2[M_v/(10^{14} M_\odot)]^{1/3}$ Mpc for our adopted cosmological model.) The errors in the parameters due to the sampling errors were found by exploring the 3-dimensional confidence region in the $M_v - \beta$, $\beta - c$ and $M_v - c$ parameter planes and finding probability contours corresponding to 1σ , 2σ and 3σ i.e. $\Delta\chi^2 = \chi^2 - \chi^2_{\min} = 3.53, 8.02, 14.2$. The best-fitting velocity dispersion and kurtosis profiles are shown in Fig. 4 and 5 as solid lines.

Interestingly, A3558 has the lowest concentration among all studied clusters. Although the rather large error bars prevent us from concluding too much, this is expected since A3558 is in the Shapley supercluster and therefore probably in the early stage of cluster-cluster mergers which destroy the inner cusp. It is also worth noting that the highest value of anisotropy ($\beta = 0.26$) is obtained for A0496 which has the highest value of line-of-sight kurtosis (see Table 1) as expected for non-rotating systems (Merritt 1987).

4.3 The mass-concentration relation

The relation between the virial mass and concentration of dark matter haloes is a well established result of N -body simulations and has been studied by many authors (e.g. NFW; Bullock et al. 2001; Dolag et al. 2004). In this subsection we address a question whether our best-fitting parameters of the clusters agree with the trend of concentration decreasing with mass as found in N -body simulations. We will compare our results to those of Bullock et al. (2001) because they used the same definition of the virial radius.

In Fig. 7 we plot estimated concentration c as a function of cluster virial mass M_v (in units of $10^{14} M_\odot$) for our six clusters. The 1σ errors following from sampling errors

of velocity moments were assigned to the points. The solid line shows the approximation of the $c(M_v)$ relation calculated from the toy model proposed by Bullock et al. (2001) which reproduces well the properties of a large sample of haloes found in their N -body simulations. The predictions were obtained for the standard cosmological model as in our simulations and $z = 0$ from their equations (9)-(13) with parameters $F = 0.001$ and $K = 3.0$ as advertised for masses $M > 10^{14} h^{-1} M_\odot$.

Although the errors in the estimated parameters are quite large it is clear from Fig. 7, that the data for clusters are consistent with the $c(M)$ relation found in N -body simulations. To make this statement more quantitative we have fitted to the data (neglecting the errors in mass) a linear relation of the form $\log c = a \log[M_v/(10^{14} M_\odot)] + b$ and found the best-fitting parameters $a = -0.6 \pm 1.3$ and $b = 1.3 \pm 1.1$ (at 68 percent confidence level). This best-fitting relation is shown in Fig. 7 as a dashed line. Therefore, although the best-fitting slope is negative, the data are also consistent at 1σ level with constant concentration or even concentration increasing with mass.

4.4 The composite cluster

The low number of galaxies per cluster in our sample results in rather large sampling errors in the measured velocity moments and therefore also large errors in the estimated parameters of the clusters. In order to reduce the uncertainties and study a typical cluster we have combined the position and velocity data for our six objects to create a composite cluster. We have normalized the galaxy distances by the estimated virial radius of their cluster, and the velocities by the circular velocity at the virial radius $V_v = \sqrt{GM_v/r_v}$. In this way we make the velocity moments independent of the virial mass. The normalized velocities and velocity moments (calculated with 121 galaxies per bin) for the composite cluster made of 1465 galaxies are shown in Fig. 8. The kurtosis-like variable is now $k = [\log(3K/2.90)]^{1/10}$ where the coefficient 2.90 was adjusted to the number of galaxies per bin. The combined samples of galaxies were those after removal of interlopers in each cluster, but we perform the procedure (fitting velocity dispersion profile and adjusting concentration while keeping $\beta = 0$) again on the total sample and it turns out that two more interlopers have to be removed. The two galaxies have been marked as before with open circles in the upper panel of Fig. 8. The two solid lines in this panel plot the last iteration of $\pm 3\sigma_{\text{los}}(R)$ profiles separating the interlopers from the galaxies included as members of the cluster.

With the mass dependence factored out, the velocity moments of the composite cluster depend only on two parameters: concentration c and anisotropy β . We adjust the parameters first by fitting only the velocity dispersion profile. The best fit is then at $c = 2.1$ and $\beta = 0.34$ with $\chi^2_{\text{min}}/N = 6.4/9$. The 1σ , 2σ and 3σ probability contours corresponding to $\Delta\chi^2 = \chi^2 - \chi^2_{\text{min}} = 2.30, 6.17, 11.8$ are shown in the upper panel of Fig. 9 with the dot marking the pair of best-fitting parameters. We can see that the 1σ confidence region is not restricted to the vicinity of the best fit but appears also at more negative β and larger c , towards the second local minimum at $c = 14.1$ and $\beta = -2.1$ with $\chi^2/N = 8.1/9$. Fitting both the ve-

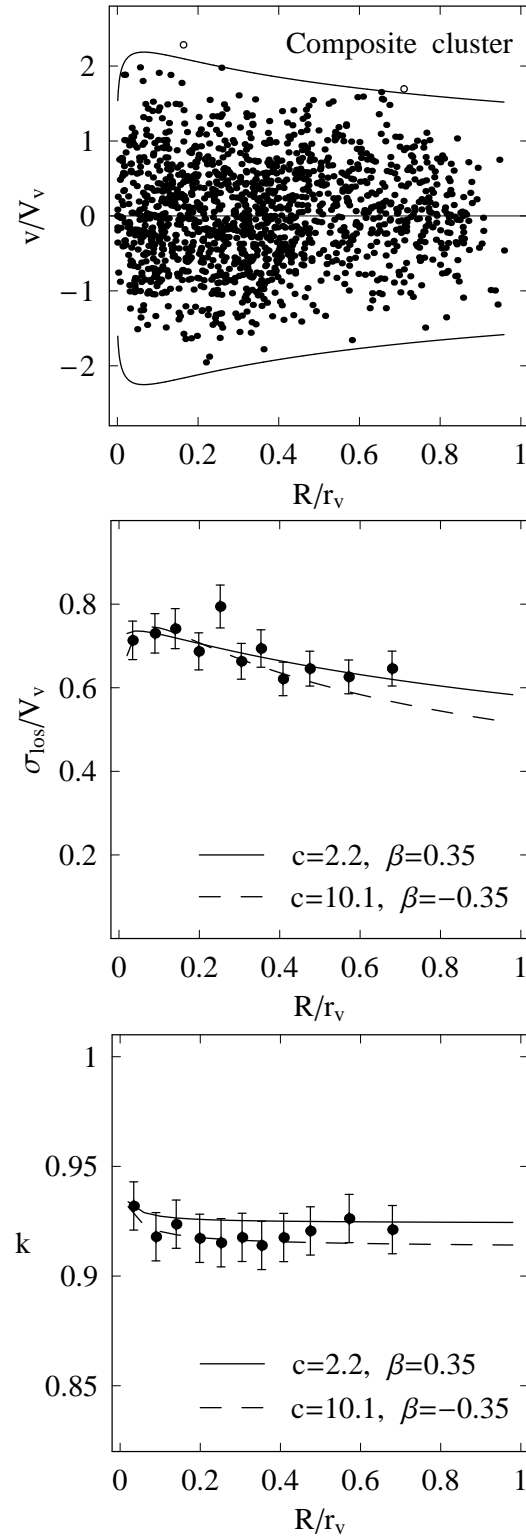


Figure 8. Upper panel: line-of-sight velocities of 1465 galaxies of the composite cluster normalized to V_v as a function of projected distance in units of the corresponding virial radius. Solid lines show fitted $\pm 3\sigma_{\text{los}}(R)$ profiles separating the galaxies included in the analysis (filled circles) from those rejected as interlopers (empty circles). Middle and lower panel: line-of-sight velocity dispersion and kurtosis profiles for the composite cluster. Solid and dashed lines show the best-fitting profiles with parameters listed in the corners of the panels.

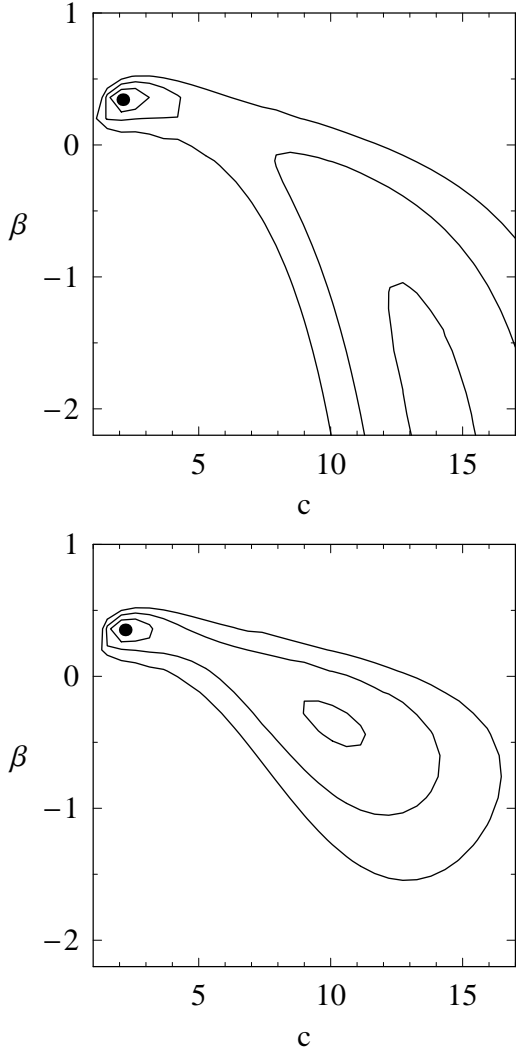


Figure 9. The 1σ , 2σ and 3σ probability contours in the $c - \beta$ parameter plane obtained from fitting the velocity dispersion only (upper panel) and both velocity dispersion and kurtosis (lower panel) of the composite cluster. The dots mark the best-fitting parameters.

larity dispersion and kurtosis breaks this degeneracy but only to some extent: the best fit is now at $c = 2.2$ and $\beta = 0.35$ with $\chi^2_{\text{min}}/N = 11.0/20$, but another local minimum of $\chi^2/N = 12.9/20$ is found at $c = 10.1$ and $\beta = -0.35$.

The presence of the two minima can be traced to the parameters estimated for each cluster separately in the last Section. In our sample we had three clusters with concentration around 3 and three clusters with concentrations of the order of 10. Those more concentrated also had lower mean value of β . Indeed, performing similar fitting for composite clusters made separately of these two groups we find single minima at $c = 1.8$ and $\beta = 0.2$ for low-concentration clusters while $c = 12.7$ and $\beta = -0.5$ for high-concentration clusters.

The profiles of the normalized moments for the best-fitting parameters are plotted as solid lines in the middle and lower panel of Fig. 8. The solutions corresponding to the second local χ^2 minimum are plotted as dashed lines. Recall, that these are best-fitting profiles obtained from the joint fit

of dispersion and kurtosis and not to each of them separately – this is why the fitted kurtosis profile does not match the corresponding data perfectly. Actually the best fit to the kurtosis data alone would have β closer to zero (isotropic orbits), but the velocity dispersion forces β towards more radial or more tangential values. Therefore, to summarize our results for the composite cluster, we find $1.5 < c < 14$ and $-1.1 < \beta < 0.5$ at the 95 percent confidence level.

5 DISCUSSION

We performed a joint analysis of velocity dispersion and kurtosis profiles of galaxies in six nearby relaxed galaxy clusters estimating two global parameters of their mass distribution and the anisotropy of galaxy orbits. The method of joint fitting the moments was tested on simulated dark matter haloes and a new procedure for interloper removal was applied. With the presently available number of galaxy redshifts per cluster the errors in the estimated parameters are still large. The estimates of mass have an error from 20 percent in the case of A0496 to 50 percent in the case of A3158 and are in rough agreement with previous estimates. The uncertainties in the estimates of concentration are even larger. The fitted parameters are consistent with the mass-concentration relation found in N -body simulations.

The method has been first applied a few years ago to the Coma cluster (Lokas & Mamon 2003) for which the largest number of galaxy redshifts is available. This larger amount of data allowed for a more detailed analysis: the dark matter distribution could be modelled separately from stars and gas, the luminosity density profile could be used as a tracer distribution without assuming that galaxies trace the total or dark matter distribution, galaxies identified as members of binaries could be removed from the sample and the analysis could be restricted to early type galaxies which are believed to be more relaxed. For the present sample of galaxy clusters we had smaller numbers of galaxies and had to simplify the analysis. However, we believe that the clusters discussed here are really relaxed which appears not to be the case for Coma (which is probably the product of a recent merger as suggested by its perturbed gas distribution and the presence of two cD galaxies). In addition, in the present study we have improved the method by introducing a reliable new procedure for the removal of interlopers.

Inclusion of kurtosis in the analysis allowed us to constrain the anisotropy and thereby break the degeneracy between the mass distribution and anisotropy present in the analysis of velocity dispersion. This led us to expect that very tight constraints on the concentration parameter and anisotropy could be obtained if the analysis was performed on a composite cluster made of galaxies belonging to all six clusters. Although the anisotropy was indeed constrained also in this case some degeneracy still persists between c and β and almost equally good fits can be found for very different pairs of the two parameters. The degeneracy may however also be due to the rather simple form of anisotropy which we assumed to be constant with radius. Although isotropic orbits ($\beta = 0$) can very well be a realistic case for virialized, mostly elliptical galaxies in clusters, our samples contained also spirals which probably are on more radial orbits (Biviano & Katgert 2004). While isotropy might be preserved

in the centre, our composite cluster may be better described by an anisotropy parameter increasing with radius. This possibility will be studied elsewhere.

The critical factor in studies of galaxy kinematics in clusters is the number of available redshift measurements. Since the number of such measurements typically does not exceed a few hundred, while the errors in the estimated parameters are mainly due to sampling errors, as we have shown, the future of such studies will probably still be in analyzing composite clusters. This does not allow however to study relations between individual objects, like the mass-concentration or mass-temperature relation. Those have been reserved, till recently, to studies based on X-ray observations. Although much tighter constraints e.g. on the concentration parameter can be obtained in this case (Pointecouteau, Arnaud & Pratt 2005), these studies rely on assumptions like the hydrostatic equilibrium and rather uncertain temperature profiles of the X-ray emitting gas. They should therefore be complemented by extensive analysis of galaxy kinematics in clusters. This may soon become possible with systematic photometric and spectroscopic surveys like WINGS (Fasano et al. 2005).

ACKNOWLEDGEMENTS

Computer simulations used in this paper were performed at the Leibnizrechenzentrum (LRZ) in Munich. EL and RW are grateful for the hospitality of Astrophysikalisches Institut Potsdam, Institut d’Astrophysique de Paris and Instituto de Astrofísica de Andalucía where part of this work was done. RW acknowledges the summer student program at Copernicus Center. This research has made use of the NASA/IPAC Extragalactic Database (NED) which is operated by the Jet Propulsion Laboratory, California Institute of Technology, under contract with the National Aeronautics and Space Administration. We have also used the LEDA database (<http://leda.univ-lyon1.fr>). This work was partially supported by the Polish Ministry of Scientific Research and Information Technology under grant 1P03D02726 as well as the Jumelage program Astronomie France Pologne of CNRS/PAN and the exchange program of CSIC/PAN.

REFERENCES

- Bardelli S., Pisani A., Ramella M., Zucca E., Zamorani G., 1998, MNRAS, 300, 589
- Basilakos S., Plionis M., Yepes G., Gottlöber S., Turchaninov V., 2005, MNRAS, in press, astro-ph/0505620
- Betancort-Rijo J. E., Sanchez-Conde M. A., Prada F., Patiri S. G., 2005, submitted to ApJ, astro-ph/0509897
- Binney J., Mamon G. A., 1982, MNRAS, 200, 361
- Biviano A., Girardi M., 2003, ApJ, 585, 205
- Biviano A., Katgert P., 2004, A&A, 424, 779
- Bullock J. S., Kolatt T. S., Sigad Y., Somerville R. S., Kravtsov A. V., Klypin A. A., Primack J. R., Dekel A., 2001, MNRAS, 321, 559
- Carlberg R. G. et al. 1997, ApJL, 485, 13
- Dantas C. C., de Carvalho R. R., Capelato H. V., Mazure A., 1997 ApJ, 485, 447
- Diemand J., Moore B., Stadel J., 2004, MNRAS, 352, 535
- Dolag K., Bartelmann M., Perrotta F., Baccigalupi C., Moscardini L., Meneghetti M., Tormen G., 2004, A&A, 416, 853
- Durret F., Adami C., Gerbal D., Pislar V., 2000, A&A, 356, 815
- Fasano G., et al., 2005, A&A, in press, astro-ph/0507247
- Fitchett M., Merritt D., 1988, ApJ, 335, 18
- Goto T., 2005, MNRAS, 359, 1415
- Horner D. J., Baumgartner W. H., Gendreau K. C., Mushotzky R. F., Loewenstein M., Molnar S. M., 2000, 197th AAS Meeting, Bulletin of the American Astronomical Society, 32, 1581
- Jones C., Forman W., 1999, ApJ, 511, 65
- Katgert P., Biviano A., Mazure A., 2004, ApJ, 600, 657
- Kazantzidis S., Kravtsov A. V., Zentner A. R., Allgood B., Nagai D., Moore B., 2004, ApJL, 611, 73
- Klypin A., Hoffman Y., Kravtsov A. V., Gottlöber S., 2003, ApJ, 596, 19
- Lokas E. L., 2002, MNRAS, 333, 697
- Lokas E. L., Hoffman Y., 2001, in Spooner N. J. C., Kudryavtsev V., eds, Proc. 3rd International Workshop, The Identification of Dark Matter. World Scientific, Singapore, p. 121
- Lokas E. L., Mamon G. A., 2001, MNRAS, 321, 155
- Lokas E. L., Mamon G. A., 2003, MNRAS, 343, 401
- Lokas E. L., Mamon G. A., Prada F., 2005a, MNRAS, 363, 918
- Lokas E. L., Prada F., Wojtak R., Moles M., Gottlöber S., 2005b, MNRAS Letters, in press, astro-ph/0507508
- Mahdavi A., Geller M. J., 2004, ApJ, 607, 202
- Mamon G. A., Lokas E. L., 2005, MNRAS, 363, 705
- Merritt D., 1987, ApJ, 313, 121
- Navarro J. F., Frenk C. S., White S. D. M., 1997, ApJ, 490, 493
- Pointecouteau E., Arnaud M., Pratt G. W., 2005, A&A, 435, 1
- Prada F., Klypin A. A., Simonneau E., Betancort-Rijo J., Patiri S., Gottlöber S., Sanchez-Conde M. A., 2005, submitted to ApJ, astro-ph/0506432
- Sanchis T., Lokas E. L., Mamon G. A., 2004, MNRAS, 347, 1198
- van der Marel R. P., Magorrian J., Carlberg R. G., Yee H. K. C., Ellingson E., 2000, AJ, 119, 2038
- Wojtak R., Lokas E. L., Gottlöber S., Mamon G. A., 2005, MNRAS, 361, L1